Exploring the Sequence of Electron Density along the Chemical Reactions between Carbonyl Oxides and Ammonia/Water Using Bond Evolution Theory

Abel Idrice Adjieufack, Maraf Mbah Bake, Charnel Nguemo Nguimkeu, Julien Pilmé, Ibrahim Mbouombouo Ndassa

Exploring the Sequence of Electron Density along the Chemical Reactions between Carbonyl Oxides and Ammonia/Water Using Bond Evolution Theory.

Abel Idrice Adjieufack[a,b*], Maraf Mbah Bake[a,b], Charnel Nguemo Nguimkeu[a,b], Julien Pilmé[c] and Ibrahim Mbouombouo Ndassa[b*]

[a]*Physical and Theoretical Chemistry Laboratory, University of Yaoundé 1, Cameroon.*
[b]*Computational Chemistry Laboratory, High Teacher Training College, University of Yaoundé 1, Cameroon.*
[c]*Sorbonne Université, CNRS, Laboratoire de Chimie Théorique, CC 137-4, place Jussieu F. 75252 PARIS CEDEX 05, France*

E-mail: adjieufack21@gmail.com ;
ibrahim.mbouombouo@univ-yaounde1.cm

Abstract

The molecular mechanism of the reactions between four carbonyl oxides and ammonia/water is investigated using the M06-2X functional together with 6-311++G(d,p) basis set. The analysis of activation and reaction enthalpy shows that the exothermicity of each process was increased with the substitution of electron donating substituents (methyl and ethenyl). Along each reaction pathway, two new chemical bonds C-N/C-O and O-H were expected to form. A detailed analysis of the flow of the electron density during their formation have been characterized from the perspective of bonding evolution theory (BET). For all reaction pathways, BET revealed that the process of C-N and O-H bond formation takes place within of four stability structural domains (SSD) which can be summarized as follows: the depopulation of V(N) basin with the formation of first C-N bond (appearance of V(C,N) basin), cleavage of N-H bond with the creation of V(N) and V(H) monosynaptic basin and finally the V(H,O) disynaptic basin related to H-O bond. On the other hand, in the case of water, the cleavage of O-H bond with the formation of V(O) and V(H) basins is the first stage, followed by the formation of the O-H bond as a second stage and finally the creation of C-O bond.

I. Introduction

One of the fundamental goals of chemistry is to describe matter at the microscopic scale in the perspective to understand its structure and to explore the mechanisms that ensure its stability. Until the beginning of the twentieth century, chemistry was essentially limited to the writing of chemical formulas for which the chemical bond was symbolized by a "trait". However, the discovery of the electron in 1897 [1] and that of the nucleus in 1911[2] have allowed the appearance of more detailed models of the atom and their mutual interactions. Among these, first model by Lewis in 1916 [3] has proposed an organization of electrons around the nuclei. This vision has been completed later by the Valence Shell Electron Pair Repulsion (VSEPR) model of Gillespie [4,5] which gave a vision of the atom for which the notion of electronic pairs is central.

Quantum mechanics have brought a rigorous description of molecular systems but at the cost of a vision relocated from the material. However, the introduction of the concept of probability density have restored this more localized vision and that of the densities of pairs have given a theoretical seat to the concept of electron pairs. From the early 1970s, Richard Bader has shown that electronic density is an important source of key information, which is obtained experimentally by X-ray diffraction spectra, or by calculation. [6,7] Its mathematical properties make it possible to divide the molecular space of rigorous way in atomic volumes. This division introduced the notion of topological atom in a molecule through the theory "Quantum Theory of Atoms in Molecules" (QTAIM), [8,9] while remaining in a purely quantum context. The atom in the molecule then has a well-defined volume and specific properties as a charge and an energy. This theory paved the way for Quantum Chemical Topology (QCT) [10,11] and its formalism has been adapted to many density functions like the ELF electron localization function of Becke and Edgecombe published in 1990.[12,13]

The ELF function measures, from a physical point of view, the increase in the spatial localization of the electron known as localization basin. Moreover, it provides a mapping method for the probability of the presence of an electron pair for a multi-electron system. Working in this sense, Kohout have proposed the Electron Localizability Indicator (ELI-D)[14,15] which is based on the motion of same spin electron density. ELI-D is an useful tool for the detection of chemical bonding signatures in molecule or crystal. [16,17] The combination of AIM and ELI-D approaches is also an issue to determine the Raub-Jansen Index (RJI) [18,19] which is an appropriate tool to describe the bond polarity. Recently, Silvi et al[20] have tried to

unify the concept of secondary bond which describes the non-covalent interactions between an acceptor molecule and an electron donor one which generally yield to complexes. They have proposed and verified by quantum calculations a set of VSEPR-inspired rules allowing the construction of bound secondary isomers($AX_{4-n}E_n$).

Although the ELF and ELI-D analyses are a well-established one-density descriptors for both covalent and non-covalent interactions,[21,22] the development of its chemical reactivity component remains a fascinating challenge. Using the electron density, Krokidis and Silvi have proposed the bonding evolution theory (BET)[23,24] which joins the electronic localization function (ELF)[24,25] with the Thom's catastrophe theory (CT).[26] BET has become a powerful tool to monitor the electronic changes or reorganization of electron pairs occurring along the reaction paths. [11, 27-32]

Research on chemical reactivity has moved from the analysis of the stationary points to the potential energy surface. In this context, a new mechanistic methodology designed to identify the favorable reaction route between several reactants was recently proposed.[33,34] However, the key questions that must be addressed to understand the nature of the molecular mechanisms remain related to fundamental chemistry: the distribution and the evolution of electron density along the reaction pathway. The bonding evolution theory, based on the changes described by Thom's catastrophe theory on the electron localization function topology along a given reaction path, is capable of unambiguously identifying the main chemical events happening throughout chemical reactions,[35-41] and generating the corresponding curly arrows to describe the reaction mechanism.[42,43]

Carbonyl oxides well known as Criegee intermediates (CIs) are strong oxidizing agents formed by ozonolysis of unsaturated hydrocarbons in the atmosphere. [44] Being among these Criegee intermediates, formaldehyde oxide (CH_2OO), acetone oxide ($(CH3)_2COO$) and methyl vinyl ketone oxide (cis and trans) due to their COO functional group can react with molecules such as H_2O, CH_3OH, NO_2, NH_3 and CH_3NH_2 to form a strong hydrogen bonds.[45] Criegee intermediates being more reactive molecules and difficult to study experimentally, computational chemists have been devoted to the exploration of their chemical reactivity. Sajadi et al.[46] have explored the potential energy surface of the reaction between CH_2OO and $(CH_3)_2COO$ with dimethyl sulfide (DMS) at the M11-L/6-311++G(2d,2p) level. The authors found within of transition state theory (TST) and RRKM theory that both reactions occurred via a strong Van der Waals complexes leading to adducts with a new C-S single bond. Mallick et al.[47] have studied the reaction of N_2O with CH_2OO using M06-2X/aug-cc-pVTZ computational level. They found that the chemical reaction mechanism could proceed through

six different channels with a rate constant of $1.79x10^{-30}$ cm^3 $molecule^{-1}$ s^{-1} for a favorable reaction pathway.

The potential energy surface of the reaction between carbonyl oxides and ammonia/water explored by some authors is found in the literature. Jørgensen et al.[48] have investigated the reaction mechanism of the chemical reactions between ammonia and carbonyl oxides using B3LYP/6-311++G(2d,2p) as computational method. They have concluded that the structural rearrangement occurred with the formation of a C-N bond between nitrogen atom of ammonia and C3 carbon atom of carbonyl oxides, followed by the hydrogen atom transfer from ammonia to the terminal oxygen of carbonyl oxides (formation of O-H chemical bond). Anglada et al. [49] have studied the chemical reaction of fifteen carbonyl oxides and water in order to understand the substitution effect in the reactivity of carbonyl oxides using Density Functional Theory (B3LYP) and *ab initio* (CCSD(T), CASSCF and CASPT2) methods. For these authors, carbonyl oxides containing the electron withdrawing substituents presented a low energy barrier and reacted rapidly with water molecule, while those ones with electron donating substituents had high energy barriers and reacted slowly. In the perspective to confirm the O-H bond formation during the chemical reaction of carbonyl oxides, Chhantyal-Pun et al.[50] have performed the experimental and computational studies on reaction of CH_2OO and $(CH3)_2COO$ with NH_3 and CH_3NH_2. They found through photoionization mass spectra data that NH_2CH_2OOH and $CH_3N(H)CH_2OOH$ were the main hydroperoxide adducts experimentally observed.

For a deep understanding of the formation of C-N, C-O and O-H chemical bonds, a detailed chemical insight on the progress of the reaction between carbonyl oxides and ammonia/water (see Scheme 1) from the perspective of bonding evolution theory (BET) is examined with a focus on the determination of reaction mechanisms, and emphasizing the way of curly arrows meeting electron density transfers in chemical reaction mechanisms. In what follow, the motivation of this present work is given by answering the following questions during the BET analyzing: i) where and how charge transfer take place along the reaction progress? how electron density rearranges and how this rearrangement can be associated with chemical events such as the breaking/forming of chemical bonds, along the reaction progress? iii) how could the electronic reorganization proceed along the reaction path? which type of catastrophe appears along each reaction pathway during the BET? iv) how is the nature of the chemical mechanism along the reaction pathway, concerted or stepwise? v) which chemical bond between C-N/C-O and O-H is formed first along each reactive pathway?

II. Theory

In quantum chemical topology, the properties of one-density scalar functions are used for discussing the nature of chemical bonding in molecules and solids.[11,51] This approach provides a partition of the function into non-overlapping atomic regions so-called basins. The gradient field is characterized by its critical points (where $\nabla\rho(\mathbf{r}) = \mathbf{0}$) and their connectivity. Critical points can be either local maxima, minima or saddle points. In the QTAIM approach, the topological atom is defined as the union of a nucleus and of its basin. Among the saddle points, a *bond critical point* (BCP) has a crucial role because, the values of some descriptors at the BCP are related to the nature of the chemical bond. The electron density at the BCP, ρ_b, is typically larger than 0.20 e bohr^{-3} in *shared-shell* interactions, in other words, covalent bonds, and smaller than 0.10 e bohr^{-3} in *closed-shell* interactions (*e.g.* ionic, van der Waals or hydrogen bonding). When the Laplacian of the density at the BCP, $\nabla^2\rho_b$, is negative, the local concentration of charge indicates a shared-shell interaction. In contrast, if $\nabla^2\rho_b$ is positive there is a depletion of charge typically characterizing a closed-shell interaction. Another descriptor often used in QTAIM to differentiate two shared-shell and closed-shell bonding scheme is the ratio $|V_b|/(2G_b)$, based on the potential energy density (V_b) and the kinetic energy density (G_b) at the BCP.[52] When this ratio is smaller than 1, the kinetic energy density is the leading term and electrons are destabilized close to the BCP, thus no covalency is expected (for example pure ionic or van der Waals bonding).

Another scalar field is the Electron Localization Function (ELF) which is a measure of the possibility of finding an electron in the vicinity of a reference electron at a given point with the same spin. [12] It was set up by the original formulation of Becke and Edgecombe and defined as follows:

$$\eta(r) = \frac{1}{1+\left(\frac{D_\sigma(r)}{D_\sigma^0(r)}\right)^2} \qquad (1)$$

The equation (1) lies on the conditional same-spin pair probability $D_\sigma(r)$ scaled by the homogeneous electron gas (HEG) kinetic energy density $D_\sigma^0(r)$,

$$D_\sigma(r) = \tau_\sigma(r) - \frac{1|\nabla\rho_\sigma|^2}{4\,\rho_\sigma(r)} \qquad (2)$$

$$D_\sigma^0(\mathrm{r}) = \frac{3}{5}\,(6\pi)^{2/3}{\rho_\sigma}^{5/3}(r) \qquad (3)$$

ELF ranges from 0 to 1 where 1 is a situation void of Pauli repulsion, i.e. a high probability of finding electron localization. A few years later, this formulation has been generalized to the

DFT theory by Savin and co-workers, [13] and rationalized in terms of the local excess kinetic energy due to the Pauli repulsion.

The usefulness of the electronic localization function is mainly due to the way it allows the analysis of the electronic localization in a very chemically intuitive way. During this ELF analysis, the reaction pathway is divided into domains (basins) where the presence is maximal to find an electron paring.[12,22] Following the chemical intuition, two types of basins can be itemized: core and valence basins. The second one is classified into their synaptic order *i.e.* the number of core basins with which they share a common boundary [53]: protonated basin denoted V(A,H), monosynaptic basin for a lone pair [V(A)] and disynaptic basin [V(A,B)] for a bonding region between two (A and B) or several nuclei. The basin populations are then obtained from the usual condensation of the electron density computed over the ELF basin volumes.

Relative to the position changes of different structural stability domain (SSD) found during the BET analysis for a given reaction pathway, we have proposed to evaluate the synchronicity of chemical process by defining the synchronicity indicator. [54,55] Its expression is given by equation (4).

$$S_y = 1 - \frac{2}{n(n-1)\left(S_f - S_0\right)} \sum_{i=1}^{n} \sum_{j=i+1}^{n} (S_j - S_i) \qquad (4)$$

In equation (4), n is the number of SSD found along the BET and S_f and S_o are the final and initial IRC coordinates values. In addition, S_j and S_i represent the different values of IRC between appeared SSDs. The maximum value of S_y amounts to 1 and its minimum value can be expressed as followed:

$$S_y^{min} = 1 - \frac{2\left(\sum_{i=1}^{n}(n-i) - \sum_{i=1}^{n/2}(n-2i)\right)}{n(n-1)} \qquad (5)$$

The absolute synchronicity (S_y^{abs}) can be derived from equation (**4)** and (**5)** as:

$$S_y^{abs} = \frac{S_y - S_y^{min}}{1 - S_y^{min}} \qquad (6)$$

III. Computational Method

Full geometries optimizations have been performed with the aid of Gaussian 16 program.[45] The electronic structures as well as the geometries of the reactants, products, and transition states have been determined at the M06-2X functional [46] using 6-311++G(d,p) basis set. The transition states TSs were further confirmed by vibrational analysis and

characterized by the only one imaginary vibrational mode. The IRC curves [47,48] were calculated following the path of reactant to the product using a standard integration method. [49] To perform the ELF topological analysis within the BET theory, the wave function was obtained for each point of the IRCs. The ELF analysis was performed with the aid of TopMod package [50] by considering a cubic grid of 0.2 bohr. Finally, ELF basin positions were visualized using Drawmol [51] while electron population evolution of basins along the IRC was done with Drawprofile.[52]

The QTAIM analysis was performed using the TopChem2 package [53] while the ELF basin isosurfaces were also displayed with Drawprofile [52] software.

IV. Results and discussion

1. Energetical, structural and QTAIM analysis

Scheme 1 displays the stereochemical structures of the different carbonyl oxides **1-4** and their corresponding reaction with ammonia and water, yielding to alkylamines, (**1-4**)**a** and hydroxyalkyl α-hydroperoxides, (**1-4**)**b** respectively. The reaction *channel-a* represents the reaction of carbonyl oxides **1-4** with ammonia while *channel-b* describes the one of water.

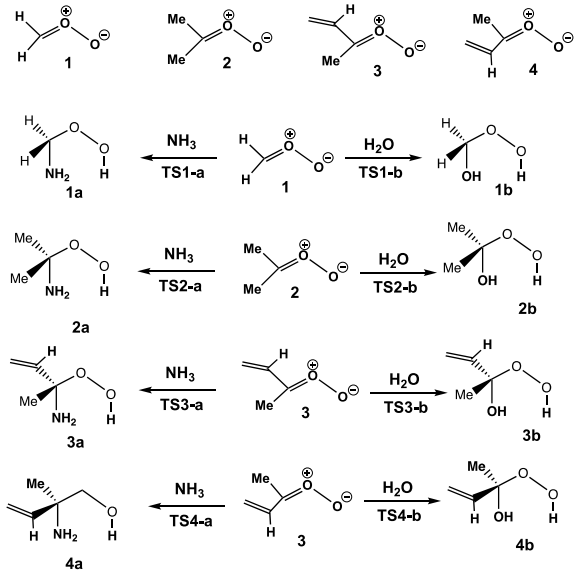

Scheme 1. Structure of carbonyl oxides **1-4** and their corresponding reaction pathways with ammonia [**TS(1-4)a**] and water [**TS(1-4)b**].

- ***Reaction carbonyl oxides 1-4 with ammonia***

Table 1 displays the activation energies of the different species engaged in reaction of carbonyl oxides with ammonia and water. The activation barrier of **TS1-a** for the carbonyl oxide **1** with ammonia is 0.9 kcal/mol. Firstly, when the two hydrogen atoms of carbonyl

oxide **1** are substituted by two methyl groups in the perspective to form carbonyl oxide **2**, the activation energy arising from this substitution is 7.1 kcal/mol. This activation barrier is 6.2 kcal/mol higher than **TS1-a.** Secondly, one methyl group of dipole **b** is replaced by ethenyl one, two carbonyl oxides namely **3** and **4** are possible with the different (*Z* and *E*) positions of ethenyl group. Compared to the reaction of carbonyl oxide **1**, they present an activation energy gap of 5.9 and 7.7 kcal/mol. With respect to the activation energy, the reaction of carbonyl oxide **1-4** with ammonia are very much influenced by the presence of the substituents at the carbonyl oxide framework and playing a key role on the reactivity of carbonyl oxides. Furthermore, the reaction activation energies follow the same tendency with the activation energy of adduct **1a** which is 11.9, 13.2 and 15.1 kcal/mol lower than the ones of adducts **2a**, **3a** and **4a**, respectively.

Table 1. The relative (ΔE°, in kcal/mol) activation energies and thermodynamics parameters (ΔH° and ΔG°, in kcal/mol and ΔS°, in cal/mol.K) of the different complexes engaged in reaction of carbonyl oxides with ammonia and water computed at 25°C with M06-2X/6-311++G(d,p) level of approximation.

Species	**ΔE°**	**ΔH°**	**ΔS°**	**ΔG°**
TS1-a	0.9	0.7	-6.3	2.6
TS2-a	7.1(6.2)	6.9(6.2)	-9.8(-3.5)	9.8(7.2)
TS3-a	6.7(5.9)	6.3(5.5)	-9.7(-3.4)	9.2(6.6)
TS2-a	8.6(7.7)	8.2(7.5)	-10.4(-4.1)	11.4(8.8)
TS1-b	7.4	6.7	-8.6	9.3
TS2-b	12.9(5.6)	11.5(4.8)	-9.2(-0.6)	14.3(5.0)
TS3-b	12.8(5.5)	11.0(4.3)	-10.1(-1.4)	14.0(4.7)
TS4-b	14.4(7.0)	12.7(5.9)	-10.0(-1.4)	15.6(6.3)
1a	-46.7	-46.6	-7.8	-42.3
2a	-34.8(11.9)	-33.1(11.5)	-10.7(-2.9)	-29.9(12.4)
3a	-33.5(13.2)	-32.(12.4)	-10.7(-2.9)	-29.1(13.2)
4a	-31.6(15.1)	-30.2(14.4)	-10.8(-3.0)	-27.0(15.3)
1b	-43.3	-41.0	-6.7	-39.0
2b	-31.3(11.9)	-29.7(11.3)	-8.7(-2.0)	-27.1(11.9)
3b	-29.3(14.0)	-28.0(13.0)	-8.8(-2.1)	-25.4(13.6)
4b	-27.2(16.1)	-25.8(15.2)	-8.0(-1.3)	-23.4(15.6)

Thermodynamics parameters (relative enthalpies, entropies and Gibbs free energies) are also reported in Table 1. As activation energy, the activation enthalpy and free Gibbs energy follow the same tendencies. For those of reaction, the enthalpy is negative, suggesting an exothermic process for these chemical reactions between carbonyl oxides with ammonia. Furthermore, the substitution of the two hydrogen atoms by methyl and ethenyl groups increases the exothermicity with an enthalpy energy of product **1b** is 11.5, 12.4 and 14.4 kcal/mol lower than **2b**, **3b** and **4a**, respectively.

- ***Reaction between carbonyl oxides 1-4 with water.***

The relative activation energies, relative enthalpies, entropies and Gibbs free energies of all stationary points engaged in the reaction between carbonyl oxides **1-4** and water are also reported in Table 1. **TS1-b** presents an activation energy which is 5.6, 5.5 and 7.0 kcal/mol lower than the **TS2-b**, **TS3-b** and **TS4-b,** respectively. This analysis of activation energy allows us to conclude that the substitution of carbonyl oxide **1** by the electron donating substituents (methyl and ethenyl) increases the activation barrier. This is also verified for the reaction energy with product **1b** which is 11.9, 14.0 and 16.1 kcal/mol more than those of **2b**, **3b** and **4b**, respectively.

Concerning the thermodynamics parameters, as for the case of ammonia, the enthalpy energy is also negative, suggesting an exothermic character in the formation of products.

- ***Analysis of structural parameters***

The structures of transition states (TSs) are represented in Figures 1 and 2. The bond lengths of O1-H1 and C3-N4 at **TS1-a** are 2.139 and 2.188 Å, respectively (Figure 1). The substitution of hydrogen atoms of the dipole **1** by methyl groups, allows a decrease in O1-H1 and C3-N4 length at **TS2-a** by 0.191 and 0.186 Å, respectively. In the cases of **TS3-a** and **TS4-a**, the same phenomenon is observed when one methyl group of carbonyl oxide **2** is replaced by ethenyl. **TS3-a** and **TS4-a** present the shortest lengths of O1-H1 (1.924 Å at **TS3-a** and 1.908 Å at **TS4-a**) forming bonds compared to first two transitional states. This bond shortening can be explained based on steric hindrance around the carbon C3 of the carbonyl oxides.

Figure 2 shows the structures of TSs involved in the reactions between carbonyl oxides and water. Compared to Figure 1, Figure 2 reveals that the replacement of ammonia molecule by water has a great effect on the geometrical structure of transition state (TSs). In fact, the length of O1-H1 and C3-O4 forming bonds are shorter than those in the case of reactions between carbonyl oxides and ammonium.

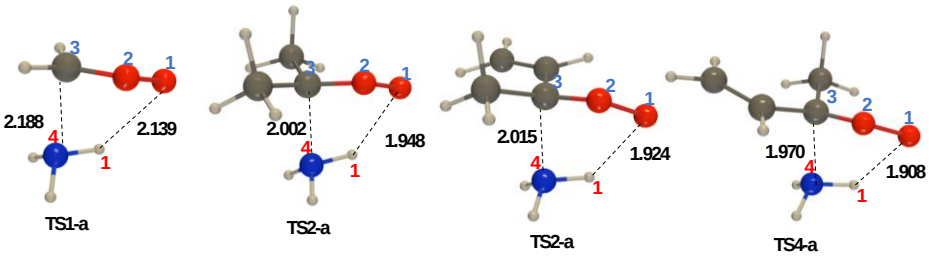

Figure 1. M06-2X/6-311++G(d,p) optimized geometries for the TSs involved in these reactions between carbonyl oxides and ammonia with indicated bond distances.

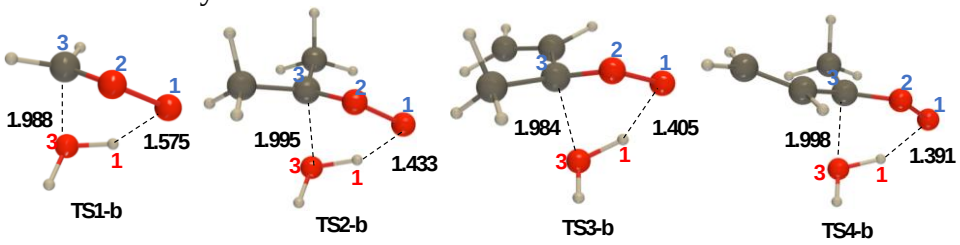

Figure 2. M06-2X/6-311++G(d,p) optimized geometries for the TSs involved in these reactions between carbonyl oxides and water with indicated bond distances.

- ***QTAIM analysis of TS structures***

We now continue with a QTAIM analysis for the both TS series. As shown in Table 2, two new bond critical points have been identified, first between H1 and O1 and second, between C3 and N4 in the case of ammonia and C3 and O4 in the case of water, respectively. These results reveal a typical signature of the formation of the two emerging chemical bonds. As observed in Table 2, the atomic charge of the H1 atom varies between 0.45e to 0.51e along the TS(1-4)a series while H1 displays a charge upper than 0.63e along the TS(1-4)b series. In addition, since some covalency is witnessed by the $|V_b|/G_b$ ratio that is always greater than 1, (*i.e.* the potential energy density dominates and electrons are stabilized at the BCP), the O1-H1 emerging bond seems to be easier triggered in the TSb series (ratio upper than 1.0) than in the TSa series (ratio lower than 1.0). Therefater, the QTAIM analysis shows that, along the TS2 series, by going from the TS1-b structure to the TS4-b ones, the covalent character of the H1-O1 and C3-N4/O4 bonds is reinforces since ρ_b and the $|V_b|/G_b$ values increase while the $\nabla^2\rho_b$ ones tends to decreased. The same trends are observed for the TS(1-4)a series. In summary, these latter results are perfectly consistent with the increase of relative activation energies observed along the carbonyl oxides series from TS1-b to TS4-b structures.

Table 2. Selected QTAIM descriptors (in a.u.) obtained at M06-2X/6-311++G(d,p) level of theory for the O1-H1 and C3-N4/O4 interactions involved in the TS systems.

	QTAIM charges		Descriptors at the O1-H1 BCP			Descriptors at the C3-N4/O4 BCP		
	q(H1)	q(N4) or q(O4)	ρ_b	$\nabla^2\rho_b$	$\|V_b\|/G_b$	ρ_b	$\nabla^2\rho_b$	$\|V_b\|/G_b$
TS1-a	0.45	-1.07	0.019	0.069	0.901	0.051	0.102	1.205
TS2-a	0.48	-1.06	0.029	0.101	0.962	0.077	0.088	1.488
TS3-a	0.51	-1.06	0.031	0.108	0.968	0.076	0.089	1.471
TS4-a	0.49	-1.05	0.032	0.108	0.982	0.083	0.080	1.551
TS1-b	0.65	-1.16	0.069	0.128	1.395	0.069	0.144	1.256
TS2-b	0.64	-1.15	0.099	0.105	1.625	0.070	0.133	1.286
TS3-b	0.63	-1.14	0.106	0.095	1.679	0.072	0.132	1.304
TS4-b	0.63	-1.14	0.109	0.085	1.720	0.071	0.132	1.296

2. BET Analysis

- **BET Analysis for the reaction between carbonyl oxides 1-4 with ammonia.**

The mechanism of the reaction between carbonyl oxide 1 and ammonia

To further clarify the bond formation/breaking process, the analysis of ELF topology (BET) along the reaction path between carbonyl oxide **1** and ammonia is studied. The BET study shows clearly a total of four structural stability domains (SSD) are recorded as displayed in Figure 3.

The first domain (SSD-I) displays the ELF basin populations of the two reactants as reported in Table S2(SI). In the framework of carbonyl oxide **1**, these basins are highlighted as follows: two monosynaptic basin V(O1) and V(O2) with a total population of 6.23 and 3.41e, and two disynaptic basins V(O2,C3) and V(O1,O2) integrating respectively 2.78 and 1.01e. The ammonia shows four basins related to N4 lone pair [V(N4) with 2.05e] and N-H bonds [V(H1,N4) with 1.96e, V(H2,N4) and V(H3,N4) integrating 1.92e each one]. At the end of domain, some basins such V(N4), V(O1,O2) and V(O2,C3) present a decrease of 1.69, 0.81 and 2.09e in theirs electronic populations.

The decrease of V(N4) population continues along SSD-II domain with its disappearance in favor of the formation of new basin disynaptic basin V(C3,N4) as can be seen in Figure 4 and in Scheme 2. This new basin V(C3,N4) represents the first main topological change and illustrates the formation of C3-N4 bond. Its population of 1.73e corresponds almost to the electron population of the former monosynaptic basin V(N4) at the end of first domain.

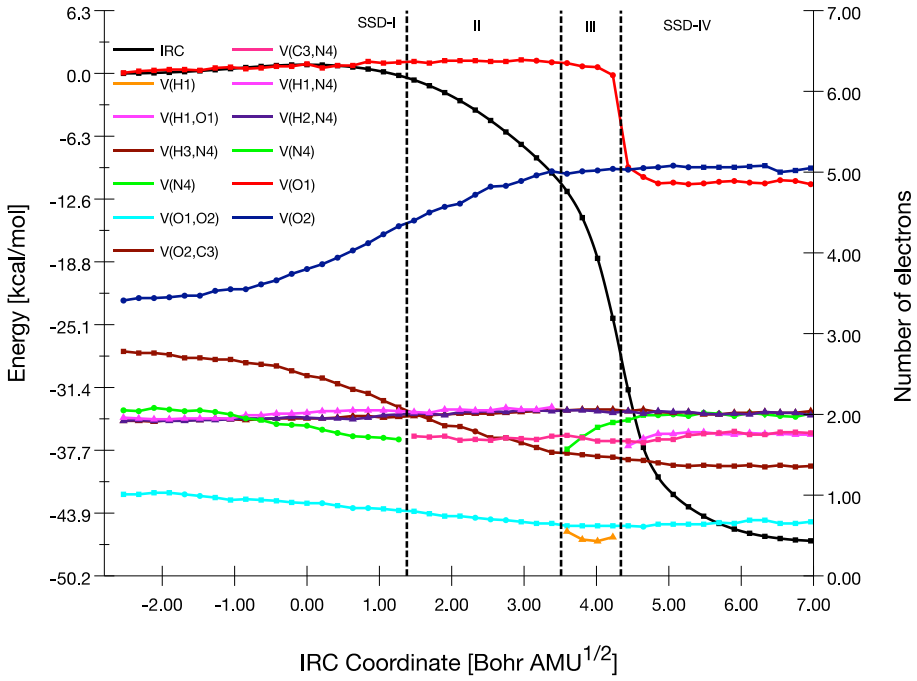

Figure 3. Evolution of electron population (in e) of selected basins engaged in the formation of O1-H1 and C3-N4 bonds along the **TS1-a** reactive pathway.

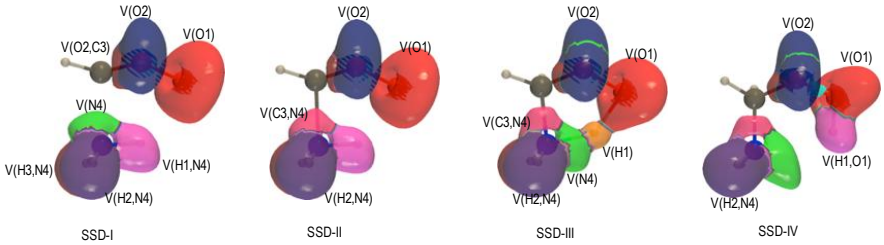

Figure 4. ELF basin isosurfaces (η=0.7) of each of the SSD recorded and engaged in the formation of O1-H1 and C3-N4 bonds along the **TS1-a** reactive pathway.

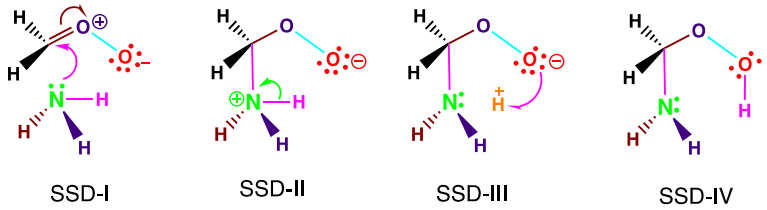

Scheme 2. Lewis structures for each SSD found along the reaction between carbonyl oxide 1 and ammonia.

Contrary to SSD-II with formation of C3-N4 bond, the third domain (SSD-III) exhibits two new monosynaptic basins [V(H1) and V(N4)] (see Figure 4) coming from the cleavage of H1-N4 bond [disappearance of V(H1,N4) basin with a population of 2.09e at the end of SSD-III domain]. The two V(H1) and V(N4) fold catastrophes start with a population of 0.55 and 1.57e, respectively at the beginning of the domain. The appearance V(N4) around the N4 nitrogen atom represents the restoration of the lone pair N4 that was involved in the formation of the carbon-nitrogen bond (C3-N4) at the SSD-II.

Finally, the last topological change occurs along the domain SSD-IV with the formation of last chemical bond H1-O1 via the creation of V(H1,O1) disynaptic basin. The V(H1,O1) basin begin with population of 1.61e and reaches 1.75e at the end of domain. Its population comes from the disappearance of V(H1) with 0.42e at the end of third domain and the reduction of V(O1) population by 1.14e at the beginning of domain.

The synchronicity (S_y) and absolute synchronicity (S_y^{abs}) have been evaluated using the equations 4-6 and their values are: S_y=0.79 and S_y^{abs}=0.65. This value of absolute synchronicity confers a synchronous character at 65% for topological changes taking place along the reaction path **TS1-a**.

- ***The mechanism of the reaction between carbonyl oxides 2-4 and ammonia***

Like the **TS1-a** reaction path, the BET analysis was also performed along the **TS2-a**, **TS3-a** and **TS4-a** pathways associated with the reactions between carbonyl oxides **2-4** and ammonia. The number of SSD recorded along each pathway remains four as the case of **TS1-a.** Figures SI1-3 represent the evolution of electron density of selected basins engaged in the formation of H1-O1 and C3-O3 bonds while figures SI4-6 contain the ELF basin isosurfaces representation found in each SSD and Scheme SI1 illustrates the Lewis structure for each SSD. The substitution of the hydrogen (carbonyl oxide **1**) by the methyl and ethenyl group does not affect the number of SSD recorded but influences the reaction coordinate of appearance of the main topological changes. In the case of **TS2-a**, the appearance of V(C3,N4) and V(O1,H1) basins occur at the reaction coordinate Rx=0.42 and 3.13 bohr.amu$^{1/2}$ respectively, with an advance of 1.06 [V(C3,N4)] and 1.30 [V(O1,H1)] bohr.amu$^{1/2}$ compared to **TS1-a**. For the cases of **TS3-a** and **TS4-a**, the same phenomenal is also observed with an advance of 1.27 and 1.27 bohr.amu$^{1/2}$ for V(C3,N4) appearance. The V(O1,H1) disynaptic basin takes place also with an advance of 1.31 bohr.amu$^{1/2}$ at **TS3-a** and 1.45 bohr.amu$^{1/2}$ at **TS4-a**. In spite of this difference in the reaction coordinate of appearance for the V(C3,N4) and V(O1,H1) basins, the electron population are similar at the beginning of topological domains.

The estimated value of synchronicity (S_y) and absolute synchronicity (S_y^{abs}) are: 0.85, 0.83 and 0.87, and 0.76, 0.72 and 0.79 for **TS2-a**, **TS3-a** and **TS4-a,** respectively. Compared to **TS1-a,** the topological changes take place along these **TS2-a**, **TS3-a** and **TS4-a** reactive pathways with a very synchronous character.

- ***BET Analysis for the reaction between carbonyl oxides 1-4 with water.***

The mechanism of the reaction between carbonyl oxide 1 and water.

Like the reaction between carbonyl oxides **1-4** with ammonia, we have also explored the ones with water. Figure 5 displays the evolution of electron population along the reaction carbonyl oxide **1** and water. From this figure 5, the molecular chemical mechanism is divided into three domains (SSD) through the BET analysis. As in the case of ammonia, the first domain SSD-I contains the main basins of different atoms engaged in the formation of the two new O1-H1 and C3-O3 bonds. We have three basins for water molecule: V(H1,O3), V(H2,O3) and V(O3) integrating 4.51, 1.71 and 1.70e, respectively (Table SI7). The carbonyl oxide **1**, in the case of ammonia presents the same basins (with almost the same populations) which are: V(O1), V(O2), V(O1,O2) and V(O2,C3) with 6.18, 3.34, 1.05 and 2.82e, respectively.

Contrary to **TS1-a**, the second domain SSD-II corresponds here to the cleavage of H1-O3 via the transformation into V(H1) and V'(O3) monosynaptic basins as we can see in Figure 6. The V'(O3) monosynaptic basin with 1.49e corresponds to the creation of a lone pair around the O3 oxygen atom and conferring a negative charge on this atom (Scheme 3), while V(H1) monosynaptic basin with 0.41e belongs to hydrogen with positive charge. Furthermore, the last domain SSD-III corresponds to the double appearance of cusp catastrophe for the two main topological changes specifically O1-H1 and C3-O3 bonds. The population of the new basins V(H1,O1) and V(C3,O3) disynaptic basins starts with 1.67 and 0.76e and grows up to 1.75 and 1.39e. The V(H1,O1) population comes from the disappearance of V(H1) and the reduction of V(O1) monosynaptic basin population. At the beginning of the domain, the V(O1) recorded a loss of 1.27e for H1-O1 forming bond while the V(O3) disynaptic basin also recorded a loss of 0.44e for the second C3-O3 forming bond. The higher population contribution of V(C3,O3) basin comes from the disappearance of the second V'(O3) which possessed a population of 1.88 e at the end of the second domain SSD-II. Furthermore, this disappearance of V'(O3) basin also increases the electron population of V(O3) which reaches at 4.62e.

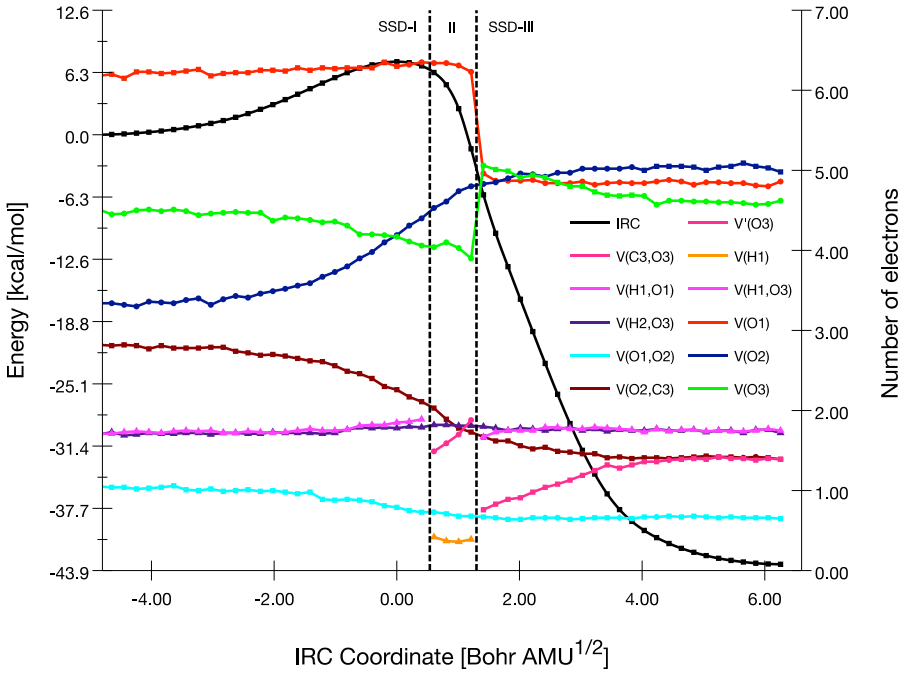

Figure 5. Evolution of electron population (in e) of selected basins engaged in the formation of O1-H1 and C3-O3 bonds along the **TS2-a** reactive pathway.

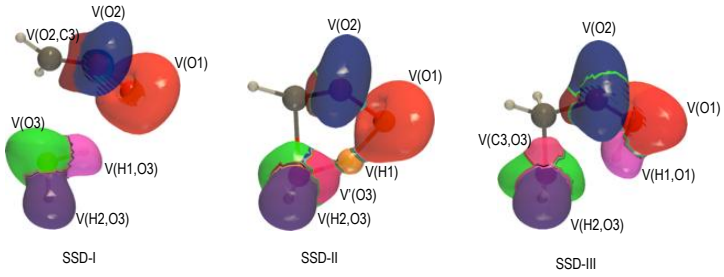

Figure 6. ELF basin isosurfaces (η=0.7) of each of the SSD recorded and engaged in the formation of O1-H1 and C3-N4 bonds along the **TS2-a** reactive pathway.

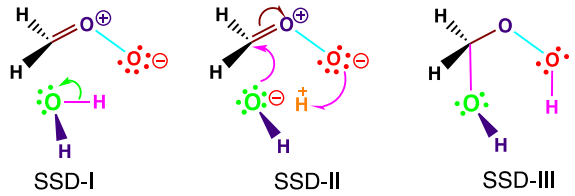

Scheme 3. Lewis structures for each SSD found along the reaction between carbonyl oxide 1 and water.

By evaluating the degree of synchronicity of the process of topological changes taking place along the pathway **TS2-a**, the calculated value of synchronicity and absolute synchronicity are: S_y=0.93 and S_y^{abs}=0.89. This value of S_y^{abs} indicates that the process takes place very synchronously and at 89% of the maximum absolute synchronicity.

- ***The mechanism of the reaction between carbonyl oxides 2-4 and water.***

The substitution of the two hydrogen of carbonyl oxide **1** by methyl and ethenyl group has generated the carbonyl oxides **2-4**. The molecular mechanism of the reaction

between carbonyl oxides **2-4** and water have also been explored by analyzing the electron density along each reactive pathway [**TS(2-4)b**] with BET. Figures SI7-9 show the evolution of electron population of selected basins engaged in the formation of O1-H1 and C3-O3 bonds. Compared to the first reactive pathway **TS2-a**, an analysis of BET reveals that each reactive pathway is described by four stability structural domains (SSDs). The main difference of these three reactive pathways with one of **TS2-a** comes from the consecutive appearance of the V(O1,H1) and V(C3,O3) along the domain SSD-III and IV respectively, as we can see in Figures SI10-12 and Scheme SI2.

The value of synchronicity (S_y) evaluated along these reactive pathways are: 0.96 (**TS2-b**), 0.95(**TS2-c**) and 0.96(**TS2-d**) while those of absolute synchronicity S_y^{abs} are: 0.93, 0.92 and 0.93, respectively. Compared to **TS2-a**, the values imply that the topological changes take place along each reaction pathway with 93% (**TS2-b** and **TS2-d**) and 92% (**TS2-c**) of synchronous character.

Conclusion

The reactions between four carbonyl oxides and ammonia/water yielding to alkylamines and hydroxyalkyl α-hydroperoxides respectively, have been investigated using the M06-2X functional together with 6-311++G(d,p) basis set. The analysis of activation energy and thermodynamic parameters clearly shows that substitution of the hydrogen atom (carbonyl oxide **1**) by the electron donor groups (carbonyl oxides **2-4**) affects the latter. The exothermicity along these chemical reactions increases from the carbonyl oxide **1** to **4** due to presence of methyl and ethenyl groups on C3 carbon atom of carbonyl oxides **2-3**.

One transitional state is found for each reaction pathway with an expected formation of two new chemical bonds, C3-N4 and H1-O1 in case of ammonia, C3-O3 and H1-O1 for water respectively. For the reaction pathway TS1-a, four structural stability domains are found and the molecular mechanism can be summarized as follows : formation of C3-N4 bond coming from the sharing of the initial population of V(N4) monosynaptic basin between C3 carbon atom of dipole a and N4 nitrogen of ammonia, and yielding V(C3,N4) basin, the transfer of the V(H1,N4) basin population to the H1[V(H1)] and N4 [V(N4)] atoms in order to restore the Lewis configuration around the N4 nitrogen atom) and finally, H1-O1 bond-forming process via the creation of V(H1,O1). However, for TS1-b reaction pathway, only three structural stability domains are recorded and different steps of chemical rearrangements are: first step corresponds to the transfer of V(H1,O3) basin population to H1 and O3 atoms

while the last step deals with the creation of two new basins V(H1,O1) and V(C3,O3) which are related to H1-O1 and C3-O3 bonds.

By substituting the hydrogen atoms by methyl and ethenyl groups, three reactions pathways were also possible and their molecular mechanism was also analyzed with BET theory. In the case of ammonia, the different stages of bond formation remain the same (four SSDs) along TS2-a, TS2-a and TS4-a reactive pathways compared to TS1-a. However, in the case of water, this substitution increases the number of SSDs to four compared to TS1-b where only three was found. This main difference comes from the double appearance of new basins V(O1,H1) and V(C3,O3) at the third domain along the TS1-b, and contrary to their consecutive appearance along TS2-b, TS3-b and TS4-b.

Associated Content

Tables containing electronic energies, enthalpies, entropies and Gibbs energies for the reaction of dipoles **a-d** with ammonia/water; Electron populations for each BET analysis for reaction of dipoles **a-d** with ammonia/water; Lewis structures for each SSD found along the reaction between dipole **b-d** and ammonia/water.

Corresponding Authors

Email: adjieufack21@gmail.com and ibrahim.mbouombouo@univ-yaounde1.cm

Author Information

Abel Idrice Adjieufack: 0000-0001-8769-6036

Ibrahim Mbouombouo Ndassa :0000-0003-0714-4982

Notes

The authors declare no competing financial interest.

Acknowledgements

A.A.I. thanks the University of Namur (Belgium) for his UNamur-CERUNA Ph.D. Mobility Fellowship. Authors are gratefull to the Consortium des Équipements de Calcul Intensif (CÉCI, http://www.ceci-hpc.be) and particularly the Technological Platform of High-Performance Computing for all calculations through financial support from the FNRS-FRFC, of the Walloon Region, and of the University of Namur (Conventions No. 2.5020.11, GEQ U.G006.15,1610468, and RW/GEQ2016).

References

[1] J.J.Thomson, *London, Edinburgh, and Dublin Phil. Mag. and J. Sci.* **1897**, *44*, 293-316.
[2] E.Rutherford, *London, Edinburgh, and Dublin Phil. Mag. and J. Sci.* **1911**, *21*. 669-688.
[3] G.N. Lewis, *J. Am. Chem. Soc*. **1916**, *38*, 762-785.
[4] R.J. Gillespie and R. Nyholm, *Q. Rev. Chem. Soc.* **1957**, *11*, 339-380.
[5] R.J.Gillespie, *J.Chem. Educ.* **1963**, *40*, 295.
[6] R.F.W. Bader and W.H. Henneker, *J. Am. Chem. Soc.* **1965**, *87*, 3063-3068.
[7] R.F.W. Bader and M.E. Stephens, *J. Am. Chem. Soc.* **1975,** *97*, 7391-7399.
[8] R.F.W. Bader, *Acc. Chem. Res.* **1985,** *18*, 9-15
[9] F.W.Biegler-könig, R.F.W. Bader and T.-H. Tang, *J. Comput. Chem.* **1982**, *3*, 317-328.
[10] A.M. Pendás and E.Francisco, *J. Chem. Theo. Comput.* 2019, *15*, 1079-1088.
[11] R.Chauvin, C. Lepetit, B. Silvi and E. Alikhani (Eds.). (2016). *Applications of Topological Methods in Molecular Chemistry, Springer, Berlin.* **2016**.
[12] A.D.Becke and K.E. Edgecombe, *J .Chem .Phys.* **1990**, *92*, 5397-5403.
[13] A. Savin, O. Jepsen, J. Flad, O. K. Andersen, H. Preuss and H. G. von Schnering, *Angew. Chem. Int. Ed. Engl.* **1992**, *31*, 187
[14] M. Kohout, *Int. J. Quantum Chem*. **2004**, 97, 651-658.
[15] M. Kohout, F. R. Wagner, Y. Grin, *Theor. Chem. Acc*. **2008**, 119, 413-420.
[16] L. Checinska, S. Mebs, B. Osmiałowski, A. Zakrzewska, K. Ejsmont, M. Kohout, *Chem. Phys. Chem.* **2016**, 17, 1-13.
[17] E. Hupf, E. Lork, S. Mebs, L. Checinska, J. Beckmann, *Organometallics,***2015**, 33, 7247-7259.
[18] S. Raub, G. Jansen, *Theor. Chem. Acc*. **2001**, 106, 223-232.
[19] I. Vidal, S. Melchor, J. A. Dobado, *J. Phys. Chem. A* **2005**, 109, 7500-7508.
[20] B.Silvi, E.Alikhani and H. Ratajczak, *J. Mol. Model.***2020**, *26*, 62.
[21] J.-P. Piquemal, J. Pilmé, O. Parisel, H. Gérard, I. Fourré, J. Bergès, C. Gourlaouen, A. De La Lande, M.-C. Van Severen and B. Silvi, *Int. J. Quantum Chem.* **2008**, *108*, 1951.
[22] F. Fuster and B. Silvi, *Theor Chem Acc.* **2000,** *104*, 13-21.
[23] B. Silvi and A. Savin, *Nature* 1994, *371*, 683-686.
[24] X. Krokidis, S. Noury and B. Silvi, *J. Phys. Chem. A* **1997**, *101*, 7277-7782.
[25] A.D.Becke, *J. Chem. Phys*. **1993**, *98*, 5648-56552.
[26] R.Thom, Structural Stability and Morphogenesis, an Outline of a General Theory of Models, Benjamin/Cummings Publishing Co. *Reading, Mass.* **1980**.
[27] a)E.Cherni, A.I.Adjieufack, B.Champagne, S.Ayadi, M.Abderrabba and V.Liégeois, *J. Phys. Chem. A* **2020,** *124*, 4068-4080. b)A.I.Adjieufack, K.L.Djogang, R.B.Lekene Ngouateu, M.Mbah Bake, C.Nana Nouhou, A. Emadak, J.Ketcha Mbadcam and I.Mbouombouo Ndassa, *J. Mol. Graph. Model.* **2020**, *96*, 107513.
[28] A.I.Adjieufack, V.Liégeois, I.Mbouombouo Ndassa, J. Ketcha Mbadcam and B. Champagne, *J. Phys. Chem. A*, **2018**, *122*, 7472-7481.
[29] I.Mbouombouo Ndassa, A.I. Adjieufack, J.Ketcha Mbadcam, S. Berski, M. Ríos-Gutiérrez and L.R. Domingo, *Int. J. Quantum Chem*. **2017**, *117*, 25451.
[30] J.Andres, P. Gonzalez-Navarrete, V.S. Safont and B. Silvi, *Phys. Chem. Chem. Phys*. **2017**, *19*, 29031-29046.
[31] V.Polo, J. Andres, S. Berski, L.R. Domingo and B. Silvi, *J. Phys. Chem. A.* **2008**, *112*, 7128-7136.
[32] V.Polo and J.Andrés, *J. Comput. Chem*. **2005**, *26*, 1427-1437.
[33] J.Klein, P. Fleurat-Lessard and J. Pilmé, *J Comput Chem*. 2021, 1-15.
[34] J.Pilmé, *J. Comput. Chem.* 2017, 38, 204-210.
[35] J. Munárriz, R. Laplaza and V.Polo, *Mol. Phys.* **2019**, *117* , 1315-1324.
[36] P.González-Navarrete, J.Andrés and V.S.Safont, *Phys. Chem. Chem. Phy.* **2018**, *20*, 535-541.

[38] M.Ríos-Gutiérrez, P. Pérez and L.R. Domingo, *RSC Adv.* **2015**, *5*, 58464-58477.
[39] N.Gillet, R.Chaudret, J. Contreras-García, W.Yang, B. Silvi and J.-P.Piquemal, *J. Chem. Theo. Comput*. **2012**, *8*, 3993-3997.
[40] E.Chamorro and E. Rincón, *Theo. Chem. Acc.* **2019**, *138*, 3.
[41] A.I. Adjieufack, V. Liégeois, I. Mbouombouo Ndassa, B. Champagne, *RSC Adv*., 2021, *11*, 10083-10093.
[42] J. Andrés, L. Gracia, P. Gonzalez-Navarrete and V.S. Safont, In Quantum Chemical Topology Approach for Dissecting Chemical Structure and Reactivity, Vol. 22 Eds.: R.Chauvin, C. Lepetit, B. Silvi and E. Alikhani), *Springer, Berlin.* **2016**, pp. 257-294.
[43] J.Andrés, S. Berski and B.Silvi, *Chem. Commun*. **2016**, *52*, 8183-8195.
[44] R. Criegee, Angew. *Chem. Int. Ed.* **1975**, *14*, 745-752.
[45] a)W. Chao, C. Yin, K. Takahashi and J. Jr-M. Lin, *Phys.Chem.Chem.Phys.* **2019**, *21*, 22589-22597 b)T. Berndt, R. Kaethner, J. Voigtlander, F. Stratmann, M. Pfeifle, P. Reichle, M. Sipila, M. Kulmala and M. Olzmann, *Phys.Chem.Chem.Phys*. **2015**, *17*, 19862-19873.
[46] G. S. Sajadi, V. Saheb and S. M. Ali Hosseini, *Comput.Theor.Chem.* **2021**, *1197*, 113145-113150.
[47] S.Mallick and P. Kumar, *Comput.Theor.Chem.* **2020,** *1191*, 113023-113029.
[48] S. Jørgensen and A. Gross, *J. Phys. Chem. A* **2009**, *113*, 10284-10290.
[49] J.M. Anglada, J. Gonzalez and M.Torrent-Sucarrat, *Phys. Chem. Chem. Phys*. **2011**, *13*, 13034-13045.
[50] R. Chhantyal-Pun, R. J. Shannon, D. P. Tew, R. L. Caravan, M. Duchi, C. Wong, A. Ingham, C. Feldman,a M. R. McGillen, M. A. H. Khan, I. O. Antonov, B. Rotavera, K. Ramasesha, D. L. Osborn, C. A. Taatjes, C. J. Percival, D. E. Shallcross and A. J. Orr-Ewing, *Phys.Chem.Chem.Phys*. **2019**, *21*, 14042-14052
[51] R.F.W. Bader, *Chem. Rev.*, **1991**, *91*, 893-928.
[52] W. Nakanishi and S. Hayashi, *J. Phys. Chem. A* **2013,** *117*, 1795-1803
[53] B.Silvi, J.Mol.Struct., 2002, 614, 3-10.
[54] A.I.Adjieufack, I. Mbouombouo Ndassa, I. Patouossa, J. Ketcha Mbadcam, V. Safont, M.Oliva and J. Andrés, *Phys. Chem. Chem. Phys*. **2017**, *19*, 18288-18302.
[55] A.I. Adjieufack, M. Mbah Bake, J. Ketcha Mbadcam, I.Mbouombouo Ndassa. J. Andrés, M.Oliva and V.S. Safont, *Int. J. Quantum Chem*. **2019**, *119*, 25985.
[56]M. Frisch, G.W. Trucks, H. B.; Schlegel, G.E.Scuseria, M.A. Robb, J.R. Cheeseman, G. Scalmani, V.Barone, B.Mennucci, G.A.Petersson, et al. Gaussian 16, Revision D. 01; Gaussian Inc.; *Wallingford, CT*, **2016**.
[57] Y.Zhao and D.G. Truhlar, *Theor. Chem. Acc*. **2008**, *120*, 215-241.
[58] C.Gonzalez and H.B. Schlegel, *J. Phys. Chem*. **1990**, *94*, 5523-5527.
[59] C.Gonzalez and H.B. Schlegel, *J. Chem. Phys*. **1991**, *95*, 5853-5860.
[60] K. Fukui, *J. Phys. Chem*. **1970**, *74*, 4161-4163.
[61] S. Noury, X.; Krokidis, F. Fuster and B. Silvi, *Comput. Chem*. **1999**, *23*, 597-604.
[62] V.Liégeois, *DrawMol;* UNamur. www.unamur.be/drawmol, **2021**.
[63] V.Liégeois, *DrawProfile;* UNamur. www.unamur.be/drawprofile, **2021**.
[64] D. Kozlowski and J. Pilmé, *J. Comput. Chem.* **2011**, *32*, 3207-3217. Available at: http://www.lct.jussieu.fr/pagesperso/pilme/topchempage.html (accessed on March 23, 2021).